JACS JOURNAL OF THE AMERICAN CHEMICAL SOCIETY

Article

Cite This: J. Am. Chem. Soc. 2018, 140, 6893−6903

pubs.acs.org/JACS

Indium Catalysts for Low-Pressure CO_2/Epoxide Ring-Opening Copolymerization: Evidence for a Mononuclear Mechanism?

Arnaud Thevenon,[†] Anish Cyriac,[‡] Dominic Myers,[‡] Andrew J. P. White,[‡] Christopher B. Durr,[†] and Charlotte K. Williams*[,†]

[†]Department of Chemistry, University of Oxford, 13 Mansfield Road, Oxford OX1 3TA, United Kingdom

[‡]Department of Chemistry, Imperial College London, London SW7 2AZ, United Kingdom

Supporting Information

ABSTRACT: The alternating copolymerization of CO_2/epoxides is a useful means to incorporate high levels of carbon dioxide into polymers. The reaction is generally proposed to occur by bimetallic or bicomponent pathways. Here, the first indium catalysts are presented, which are proposed to operate by a distinct mononuclear pathway. The most active and selective catalysts are phosphasalen complexes, which feature ligands comprising two iminophosphoranes linked to sterically hindered *ortho*-phenolates. The catalysts are active at 1 bar pressure of carbon dioxide and are most effective without any cocatalyst. They show low-pressure activity (1 bar pressure) and yield polymer with high carbonate linkage selectivity (>99%) and isoselectivity (P_m > 70%). Using these complexes, it is also possible to isolate and characterize key catalytic intermediates, including the propagating indium alkoxide and carbonate complexes that are rarely studied. The catalysts are mononuclear under polymerization conditions, and the key intermediates show different coordination geometries: the alkoxide complex is pentacoordinate, while the carbonate is hexacoordinate. Kinetic analyses reveal a first-order dependence on catalyst concentration and are zero-order in carbon dioxide pressure; these findings together with in situ spectroscopic studies underpin the mononuclear pathway. More generally, this research highlights the future opportunity for other homogeneous catalysts, featuring larger ionic radius metals and new ligands, to operate by mononuclear mechanisms.

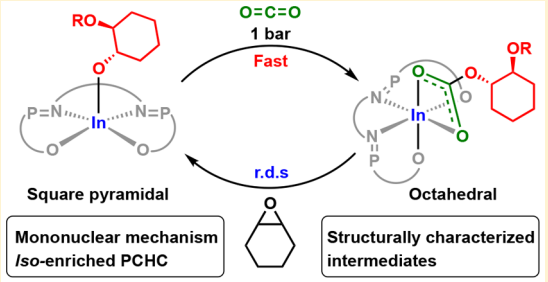

INTRODUCTION

CO_2 is a highly desirable C1 feedstock as it is abundant, inexpensive, and a common industrial and biochemical waste.[1,2] One useful way to add value to CO_2 is by its ring-opening copolymerization (ROCOP) with epoxides to produce polycarbonates.[3−9] ROCOP is particularly attractive in terms of CO_2 utilization as it is genuinely catalytic, applies low-cost commercial reagents, yields valuable products already used and sold at large-scale, and results in significant carbon dioxide uptake (CO_2 constitutes 30−50 mol % of the polymer).[10,11] The properties of the CO_2-derived polycarbonates (PC) enable them to replace conventional polymers across a wide range of applications and at large scale.[12−14] One important application is polyurethane manufacture where the PC polyols deliver equivalent properties to conventional materials and significantly reduce greenhouse gas emissions.[15−18] PCs also show promise as rigid plastics, elastomers, scratch-resistant coatings, and antimicrobial surfaces.[19−22] Nonetheless, the viability of the polymerization process remains limited by catalyst activity and scope.

The development of new catalysts requires detailed understanding of the reaction pathway(s) and is ultimately dependent upon a high selectivity for the kinetic reaction product (polymer).[5,23,24] To maximize carbon dioxide uptake, catalysts must rapidly alternate between alkoxide and carbonate intermediates; however, control over both reactivity and selectivity is not well understood. Almost all known catalysts are proposed to enchain via one of two pathways: (1) bimetallic or (2) bicomponent mechanisms, which require metal complexes to be activated by ionic or Lewis basic cocatalysts (Figure 1).[9]

Metal salen catalysts show high activity, selectivity, and polymerization control.[5−7,25−42] The most active are cobalt(III)[27−32,35,38,41−44] or chromium(III)[26,34,40,45−56] complexes, but, relevant to this work, aluminum(III) analogues show much lower activity (1 < TOF < 30 h^{-1}).[57,58] Metal salen catalysts are only highly active when applied with a cocatalyst, and equimolar catalyst:cocatalyst ratios generally work best, consistent with ion pairs being the active species (bicomponent mechanism).[36,52,59] Kinetic investigations using either Cr or Co-salen catalyst systems (i.e., metal complex + cocatalyst) show fractional orders in catalyst concentration, often between 1 and 2, consistent with a mixture of bimetallic and bicomponent mechanisms.[42,44,48] Such polymerization mechanisms bear some resemblance to bimetallic pathways invoked for metal salen catalysts in epoxide kinetic resolution.[60,61]

Received: February 15, 2018
Published: May 21, 2018

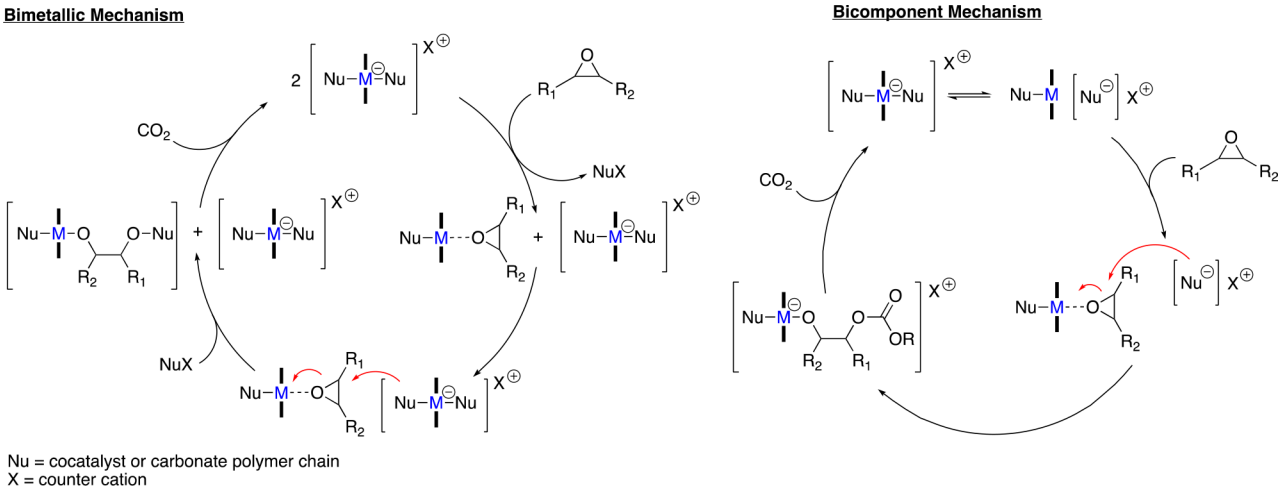

Figure 1. Two mechanisms proposed for epoxide/carbon dioxide ROCOP using metal salen catalysts. M = Cr(III)/Co(III)/Al(III), thick lines represent the salen ligand, Nu = anionic cocatalyst, e.g., Cl- or the growing carbonate polymer chain, R_1, R_2 = alkyl substituents, e.g., cyclohexylene, R = growing polymer chain.

In terms of typical operating conditions, metal salen polymerization catalyst systems usually require higher carbon dioxide pressures for optimum activity, typically at pressures from 10 to 30 bar.[5−7,25−35,37−42,44−55] The cobalt catalyst systems also require low reaction temperatures, often 25−40 °C, so as to avoid irreversible thermally activated reduction (to Co(II)); such low temperatures may be problematic for production of viscous polymers.[43,62] Despite the success of the metal salen catalyst systems, fundamental questions remain unanswered regarding the structures and reactivity of nearly all of the proposed catalytic intermediates. Understanding is hindered by a lack of isolated metal alkoxide or carbonate intermediates, uncertainties regarding whether the key intermediates are ionic or covalent compounds, the redox instability of Co(III) at higher temperatures, the paramagnetism of many intermediates, and the high CO_2 pressure requirement complicating in situ spectroscopic studies.

Motivated to address such questions, we considered that group 13 metal salen complexes could enable the use of NMR (and IR) spectroscopy to study the polymerization mechanism. Nonetheless, the low activity previously observed for Al-salen catalyst systems was discouraging, and to overcome it we targeted indium complexes. So far, indium catalysts are unknown for CO_2/epoxide ROCOP, but are catalysts for cyclic carbonate production from mixtures of epoxide and carbon dioxide.[63,64] Indium alkyl complexes are also known to undergo rapid carbon dioxide insertion;[65,66] such reactivity is potentially significant because ROCOP catalysis would require carbon dioxide insertion into indium alkoxide bonds. Indium alkoxide complexes also show greater activity in lactone ring-opening polymerization as compared to aluminum analogues;[67−69] this reactivity could be significant if the relevant indium carbonate/alkoxide intermediates in ROCOP are also more labile. In terms of ligand selection, both salen and phosphasalen indium complexes are targeted; phosphasalen ligands are analogues of salens, which feature two iminophosphoranes in place of the imines.[70] Generally, they increase electron donation to metal as compared to salens, and the phosphorus substituents provide additional steric hindrance at the active site.[71,72] Phosphasalen metal catalysts have shown high activity and control in lactide ring-opening polymerization (ROP).[70,73−75] Further, an indium phosphasalen ring-opening polymerization catalyst was considerably more active than aluminum salen analogues.[76]

RESULTS

Catalyst Synthesis and Copolymerization Studies. A series of indium phosphasalen complexes, and an analogous indium salen complex, were synthesized and tested as catalysts for cyclohexene oxide (CHO)/CO_2 ROCOP (Figure 2).

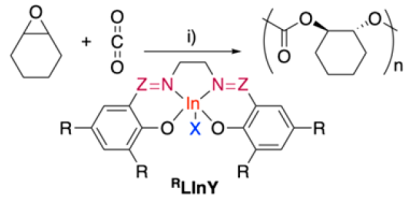

Catalyst	R	Z	X
L'InCl	^{t}Bu	C	Cl
LInCl	^{t}Bu	PPh_2	Cl
LInBr	^{t}Bu	PPh_2	Br
LInOAc	^{t}Bu	PPh_2	OAc
$LInNO_3$	^{t}Bu	PPh_2	NO_3
LInO^tBu	^{t}Bu	PPh_2	O^tBu
^{Amyl}LInO^tBu	Amyl	PPh_2	O^tBu
^{Cumyl}LInO^tBu	Cumyl	PPh_2	O^tBu

Figure 2. Ring-opening copolymerization (ROCOP) of cyclohexene oxide (CHO) and CO_2 catalyzed by indium complexes. Reagents and conditions: (i) [In] = 9.89 mM (0.1 mol % vs CHO), [CHO] = 9.89 M (i.e., neat CHO), 1 bar CO_2, 60−80 °C, 24−48 h.

The phosphasalen ligand features two phenyl substituents on the phosphorus atom, *tert*-butyl substituents at the *ortho*- and *para*-phenolate sites and an ethylene backbone linker; this same ligand was previously applied to prepare high activity lactide ROP catalysts (Figures 2 and S1−10).[76] Both the salen and the phosphasalen indium chloride complexes were synthesized by ligand deprotonation and subsequent reaction with $InCl_3$. The complexes were each isolated in high yields (>80%) (Figures S11−S17). Single crystals of the salen complex, **L′InCl**, analyzed by X-ray crystallography, show a distorted square pyramidal geometry at indium (τ_5 = 0.37).[77] The tetradentate

DOI: 10.1021/jacs.8b01920
J. Am. Chem. Soc. 2018, 140, 6893−6903

Table 1. CO_2/CHO ROCOP Catalyzed by LInCl and L′InCl, with or without Cocatalyst[a]

catalyst	cocatalyst	conversion (%)[b]	% carbonate linkages[b]	% polymer selectivity[b]	M_n[c]	$Đ$[c]
LInCl		14	66	94	197000	2.0
					7500	1.3
					700	1.2
L′InCl		21	<1	>99	416000	1.2
					10400	2.5
LInCl	PPN−Cl	8	>99	0		
L′InCl	PPN−Cl	26	>99	43	4300	1.2
LInCl	DMAP	10	>99	72	600	1.2
L′InCl	DMAP	trace				

[a]Copolymerization conditions: [cat] = 0.1 mol %, 60 °C, 48 h, where relevant [cat]/[cocat] = 1. [b]Determined by comparison of the integrals of signals arising from the methylene protons in the ^{1}H NMR spectra due to copolymer carbonate linkages (δ = 4.65 ppm) and copolymer ether linkages (only for the % polymer selectivity, δ = 3.45 ppm) against *trans*-cyclic carbonate (δ = 4.00 ppm), and *cis*-cyclic carbonate (δ = 4.67 ppm). [c]Determined by SEC, in THF, at 40 °C, calibrated using polystyrene standards. All of the data are available in Table S2.

ligand occupies the equatorial positions and the chloride the axial position. Its ^{1}H NMR spectrum (C_6D_6) confirms metal coordination by downfield shifts to all resonances as compared to free ligand and by the two multiplets assigned to the diastereotopic methylene groups. The indium phosphasalen analogue, **LInCl**, shows similar ^{1}H and ^{31}P NMR spectra, with a characteristic singlet in the ^{31}P NMR spectrum at 42.1 ppm (shifted downfield as compared to the ligand). DOSY NMR (d_8-THF, 298 K) suggests that both complexes are monomeric under conditions relevant to catalysis, an important finding given other indium halide complexes are dimeric or higher order aggregates.[78−81]

Both indium chloride complexes were tested in catalysis using a standard set of reaction conditions: neat cyclohexene oxide (9.89 M), 0.1 mol % of catalyst, 1 bar of CO_2, and 60 °C (Tables 1 and S2, and Figures S18,19). The salen catalyst produced only polyether, but the phosphasalen catalyst yielded polycarbonates with a high carbonate selectivity (94%). **LInCl** catalyzes polymer formation even at low pressures of CO_2 (1 bar), which was unexpected because other metal salen catalysts typically require much higher pressures.[7,25] Because most metal salen catalysts also require cocatalysts for high activity,[25] both catalysts were retested with the addition of an equivalent of either 4-dimethylaminopyridine (DMAP) or PPNCl (Tables 1 and S2, and Figures S17,18). The addition of DMAP severely reduced the catalytic activity, particularly evident for **L′InCl**. The addition of PPNCl completely changed the selectivity of the phosphasalen (**LInCl**), yielding only cyclic carbonate. Overall, the addition of cocatalysts was not beneficial in terms of either activity or selectivity.

The phosphasalen catalyst shows high carbonate linkage selectivity but yields multimodal molar mass distributions. This feature may be caused by relatively slow initiation from the chloride group, and to investigate further a series of phosphasalen indium complexes featuring different initiating groups were synthesized, that is, **LInX**, where X = Br, O^{t}Bu,[76] OAc, and NO_3 (Figures 2 and S20−38). Single crystals of **LInBr**, analyzed by XRD, reveal an octahedral geometry at indium, with a *trans*-phosphasalen configuration and the bromide initiating group coordinated *trans* to a THF molecule (Figure S20). To characterize the solution structure, THF was added to a solution of the complex dissolved in a noncoordinating solvent (C_6D_6). The resulting ^{1}H NMR spectrum shows only signals assigned to free THF, indicating that it is not strongly coordinated on the NMR time scale (Figure S21). DOSY NMR (d_8-THF, 298 K) confirms a monomeric structure under polymerization relevant conditions (Figure S22). Overall, the complex adopts a pentacoordinate structure similar to **LInCl** in solution (Figures S23 and 24). **LInO^{t}Bu** shows a pentacoordinate solid-state structure, with square pyramidal geometry at indium (τ_5 = 0.33, Figures 3 and S25).[76,77] The same structure is maintained in solution, and DOSY NMR suggests it remains monomeric under the conditions of catalysis (Figures 3 and S26−28).[76] In contrast, **LInOAc** and **LInNO$_3$** show distorted octahedral geometries at indium, each showing *cis*-β phosphasalen coordination modes with the acetate or nitrate ligands both adopting fully delocalized κ^2-chelation (Figures 3, S29, and S30). DOSY NMR reveals that both **LInOAc** and **LInNO$_3$** are monomeric in solution (Figures S31 and 32). The ^{1}H NMR spectra, in either C_6D_6 or d_8-THF, show three broadened resonances for the phosphorus phenyl substituents (Figure 3). The pentacoordinate indium complexes generally show five sharper resonances for the equivalent phosphorus phenyl groups (Figures 3 and S33−36). Comparing the aromatic regions, of the ^{1}H NMR spectra, of two representative compounds, pentacoordinate **LInO^{t}Bu** shows two multiplets (7.75, 7.45 ppm) for the *ortho*-phenyl protons and three multiplets for the *meta* and *para* resonances (7.09, 6.97, 6.87 ppm), whereas octahedral **LInOAc** shows a broad resonance (7.55 ppm) for the *ortho*-protons and two broad resonances (7.15 and 7.00 ppm) for the *meta* and *para* substituents (Figure 3). VT-NMR of the octahedral complex shows that the broad peaks are resolved at low temperatures to a complex series of peaks; this could be due to slow equilibration between two *cis*-β conformers, although other fluxional processes cannot be excluded (Figure S38, Scheme S5). VT-^{31}P{^{1}H} NMR shows only a single peak at all temperatures, preventing further insight. The key observation is that the ^{1}H NMR spectra of the compounds generally show characteristic chemical shifts and multiplicities for the phenyl protons, depending on whether the complex adopts a penta- or hexacoordinate structure (Figure 3).

The catalysts were each tested under the same polymerization conditions, described previously, and performances were compared to **LInCl** (Table 2, Figures S39 and 40). The bromide complex, **LInBr**, showed significantly worse performance with cyclic carbonate as the major product. Because bromide is a better leaving group than chloride, it is proposed that the first carbonate intermediate undergoes a backbiting reaction leading to cyclic carbonate formation (Scheme S6). This hypothesis is also consistent with published literature

DOI: 10.1021/jacs.8b01920
J. Am. Chem. Soc. 2018, 140, 6893−6903

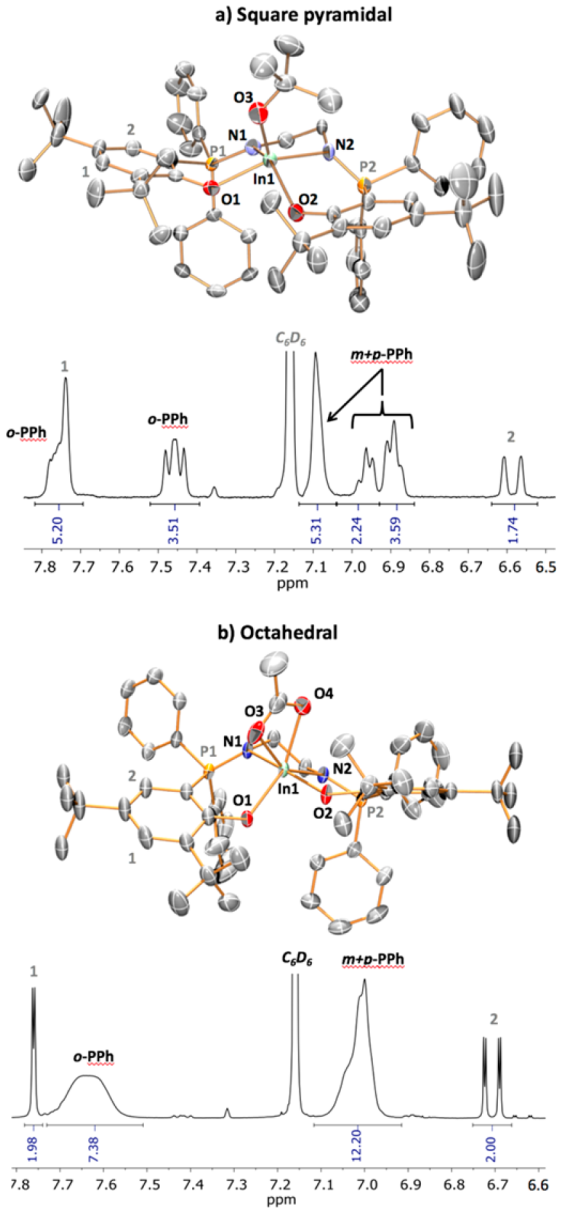

Figure 3. (a) Molecular structures and ^{1}H NMR (C_6D_6, 298 K) spectrum of **LInO^{t}Bu** (top);[76] and (b) molecular structures and ^{1}H NMR (C_6D_6, 298 K) spectrum of **LInOAc** (bottom). The molecular structures are represented with thermal ellipsoids at the 50% probability level, and ^{1}H NMR spectra are zoomed in the phenyl region (the complete ^{1}H NMR spectra and VT NMR are illustrated Figures S33 and S38).

showing that $InBr_3$ is an efficient cyclic carbonate catalyst. The alkoxide derivative, **LInO^{t}Bu**, showed much better catalytic performance yielding highly alternating polycarbonate with a high selectivity for polymer (83%). Importantly, the PC has low molar mass and a monomodal molar mass distribution, consistent with initiation and chain transfer from 1,2-cyclohexanediol (CHD) (see Discussion). MALDI-ToF mass spectra show a single series of peaks attributed to chains end-capped with hydroxyl groups (initiated from CHD, Figure S41). The acetate derivative, **LInOAc**, was almost totally inactive, and its ^{1}H NMR spectrum remains unchanged after the addition of excess epoxide and even after 2 days of heating at 60 °C (Figure S42). On the other hand, the nitrate derivative, **LInNO$_3$**, showed activity equivalent to that of **LInO^{t}Bu** but formed polymers with more ether linkages.

The phosphasalen ligand was modified at the *ortho*-phenolate to increase steric hindrance at the active site (^{amyl}**LInO^{t}Bu** and ^{cumyl}**LInO^{t}Bu**). Recently, related phosphasalen indium lactide ROP catalysts showed the highest rates for complexes with sterically hindered *ortho*-substituents; our goal was to discover if the same substituents accelerate ROCOP.[76] Two new phosphasalen indium complexes were synthesized that feature either amyl or cumyl *ortho*-phenolate substituents. The complexes show solid-state structure, ^{1}H NMR, and DOSY spectra similar to those of **LInO^{t}Bu** (Figures S43−49) and are mononuclear, pentacoordinate indium complexes under the conditions relevant to catalysis.[77] In ROCOP catalysis, ^{amyl}**LInO^{t}Bu** shows the same activity as **LInO^{t}Bu**, but ^{cumyl}**LInO^{t}Bu** is approximately twice as active (Table 2, Figures S51 and 52). All catalysts show very high selectivity for carbonate linkages (>99%). The PCs have low molar masses and monomodal distributions with narrow dispersity. Analysis of the PC ^{13}C{^{1}H} NMR spectra shows a dominant [*mmm*] tetrad resonance, which suggests the catalysts are isoselective.[82−84] The isoselectivity increases in the order **LInO^{t}Bu** (rel. intensity = 76%) < ^{amyl}**LInO^{t}Bu** (rel. intensity = 78%) < ^{cumyl}**LInO^{t}Bu** (rel. intensity = 86%) (Figures S52−54).

The stereoerrors were analyzed so as to assign the stereocontrol mechanism. In an enantiomorphic-site control mechanism, [*mrr*] and [*mmr*] tetrads are the most common stereoerrors with much smaller contributions from [*rrr*], [*rmr*], and [*mrm*] tetrads.[31] Here, the signals for [*mrr*] and [*mmr*] tetrads are absent from all spectra, which suggests a chain end control mechanism. Bernoullian statistical methods were used to calculate tetrad probabilities, and the results are close to experimental intensities suggesting a chain end control mechanism (Table S3, eq S11).[85,86]

Given the promising performance of the indium alkoxide complexes, the catalytic conditions were explored (Tables 2 and S4, Figures S55−57). The rate was more than four time higher at 80 °C, while at 100 °C high rates were observed but with reduced polymer selectivity (i.e., increased cyclic carbonate formation). The most active catalyst, ^{cumyl}**LInO^{t}Bu**, achieved a TOF of 15 h^{-1}, while maintaining high selectivity for polymer and high carbonate linkages (Table 2). Its activity is approximately equivalent to dizinc catalysts active at 1 bar pressure CO_2.[87] It also shows activity equivalent to that of aluminum salen catalysts but at a fraction of the pressure (5 < TOF < 28 h^{-1}, 34 bar of CO_2, 80 °C).[58,88] Overall, its activity is modest as compared to the most active zinc[89] or cobalt[90] catalysts in this field, but it is active at 1 bar pressure, shows high carbonate linkage and selectivity, and operates without any cocatalyst; such characteristics are valuable because they are expected to reduce costs associated with implementation.

Kinetic Studies. Kinetic analyses showed that the reaction rate (TOF) is not strongly influenced by the carbon dioxide pressure over the range 1−40 bar pressure (Figures 4, S58, 59, and Table S4). There is a slight decrease in TOF as pressure increases, but this is likely caused by increased gas expansion at higher pressures causing catalyst dilution rather than any pressure dependence.[49] These data and the catalytic activity at 1 bar CO_2 pressure signal a zero-order in carbon dioxide pressure. Several attempts to determine the order in epoxide concentration using diethylcarbonate as solvent were unsuccessful because dilution resulted only in cyclic carbonate formation (Figure S62). The order in catalyst concentration

DOI: 10.1021/jacs.8b01920
J. Am. Chem. Soc. 2018, 140, 6893−6903

Table 2. CO_2/CHO ROCOP Catalyzed by ^{R}LInX[a]

catalyst	% carbonate linkages[b]	% polymer selectivity[b]	TON	TOF (h^{-1})[c]	M_n[d] (g/mol)	$Đ$[d]	P_m[e]
LInCl	66	94	100	2	197000	2.00	
					7500	1.30	
					700	1.20	
LInBr	>99	60	20	0.4			
LInOAc	>99	85	25	0.5			
LInNO$_3$	61	80	92	2	7500	1.44	
					900	1.16	
LInO^{t}Bu	>99	83	120	2.5	1410	1.23	0.76
^{amyl}LInO^{t}Bu[f]	>99	85	140	3	1600	1.23	0.78
^{cumyl}LInO^{t}Bu	>99	90	160	3.5	2900	1.16	0.86
^{cumyl}LInO^{t}Bu[g]	>99	95	350	15	3400	1.32	

[a]R = ^{t}Bu, X = Cl, Br, O^{t}Bu, OAc, NO_3; R = amyl or cumyl, X = O^{t}Bu. Copolymerization conditions: [In] = 0.1 mol %, 60 °C, 48 h, 1 bar CO_2. [b]Determined by comparison of the integrals of signals arising from the methylene protons in the ^{1}H NMR spectra due to copolymer carbonate linkages (δ = 4.65 ppm) and copolymer ether linkages (only for the % polymer selectivity, δ = 3.45 ppm) against *trans*-cyclic carbonate (δ = 4.00 ppm), and *cis*-cyclic carbonate (δ = 4.67 ppm). [c]TON = (conversion × loading)/(100) and TOF = TON/time. [d]Determined by SEC, in THF and calibrated using polystyrene standards. [e]Determined by $^{13}C\{^1H\}$ NMR ($CDCl_3$, 125.8 MHz, Figures S53–S55). [f]80 °C. [g]80 °C, 23 h.

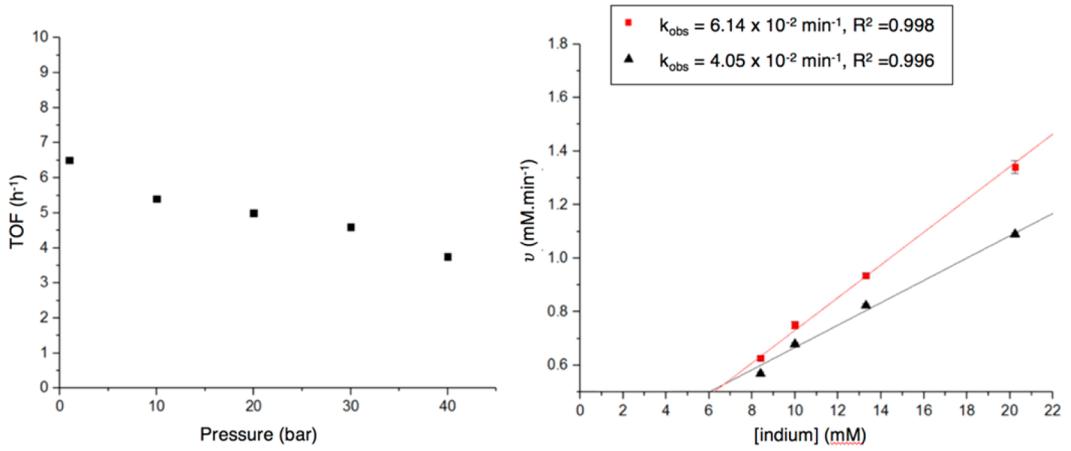

Figure 4. LHS: Plot of the catalyst activity {TOF (h^{-1})} against CO_2 pressure (bar). Polymerizations were conducted using **LInO^{t}Bu** (0.1 mol % vs epoxide), CHO (9.89 M), 80 °C, 24 h. RHS: Plot of the initial rates, k_{obs}, against catalyst concentration, [In]. The initial rates are determined using in situ ATR-IR spectroscopy by analysis of two resonances: the C═O stretch at 1787–1731 cm^{-1} (black, ▲) and a polymer mode at 1014 cm^{-1} (red, ■) (see Figure S61 for the determination of k_{obs}).

was determined by plotting initial rates, ν, over a range of catalysts concentrations (8–20 mM or 1:500–1:1250; catalyst:monomer, Figure 4). Each polymerization occurred without any significant induction period due to rapid initiation from the indium alkoxide; the lack of initiation period is different from that of many other catalysts (Figure S61).[24,26] The initial rates were monitored using in situ ATR-FTIR spectroscopy, with conversion also determined using ^{1}H NMR spectroscopy. Two characteristic IR vibrational modes were analyzed: the C═O stretch (1787–1731 cm^{-1}) and the C–O stretch (O–C═O = 1014 cm^{-1}). Initial rates were determined as the gradients of fits to conversion versus time (0–10% conversion). The order in catalyst concentration was determined from plots of initial rates versus catalyst concentration (Figure 4). In each case, the best fits are linear, which indicates a first order in catalyst concentration. Higher and lower catalyst orders were also tested, but the fits to data were clearly inferior (Figure S62). Furthermore, the plot of ln(initial rate) versus ln[indium] gave a gradient of 0.8, which is also consistent, within experimental error, with a first order in catalyst concentration (Figure S63). The plots of initial rate versus catalyst concentration were also used to determine a propagation rate constant, k_p = (5.10 ± 1.04) × 10^{-3} M^{-1} min^{-1}.

Next, the isolation and characterization of key intermediates relevant to polymerization was investigated to inform the polymerization mechanism. The stoichiometric reactions between **LInO^{t}Bu** and reagents including *trans*-1,2-cyclohexane diol (CHD), carbon dioxide, or Lewis bases were investigated. CHD was targeted because it is present as a chain transfer agent in many ROCOP reactions (see Discussion).[7,34,56,87,91–97] The reaction between 1 equiv of **LInO^{t}Bu** and CHD was monitored using ^{1}H NMR spectroscopy (Figures S64–66). As soon as the reagents were mixed, a new signal formed, which was independently assigned to *tert*-butanol. The CHD signals shifted to higher chemical shifts as compared to uncoordinated CHD. DOSY NMR analysis of the reaction mixture showed one diffusion coefficient for the phosphasalen ligand signals but distinct, mixed diffusion coefficients for the alcohols (CHD and ^{t}BuOH, Figure S67). Such features could be indicative of dynamic equilibria between different alkoxide complexes with the equilibration rates being equivalent to the DOSY NMR time scale.[98] Crystals suitable for X-ray diffraction were isolated from the reaction mixture by the slow diffusion of hexane

DOI: 10.1021/jacs.8b01920
J. Am. Chem. Soc. 2018, 140, 6893–6903

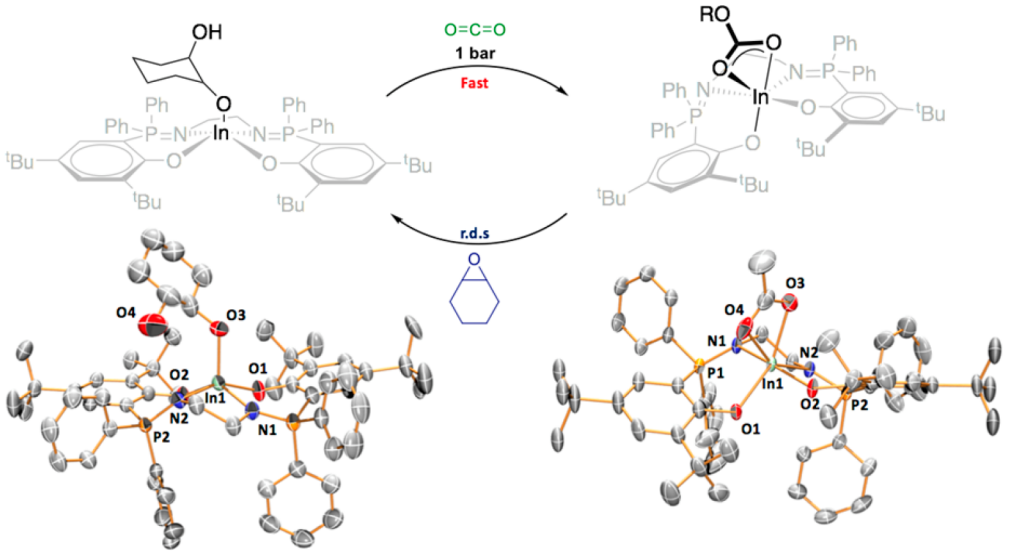

Figure 5. Schematic representation and molecular structures, with thermal ellipsoids at the 50% probability level, of two complexes relevant as catalytic intermediates: LInCHD and $LInO_2COR$. The latter molecular structure corresponds to LInOAc and is used to model the indium coordination geometry observed for the indium carbonate intermediate (vide infra). Complete data sets for the X-ray crystal structures are available in Figures S29 and S68.

(Figure 5). The solid-state structure confirms the formation of a new complex, **LInCHD**, which is an indium−alkoxide complex with monodeprotonated CHD [In−O = 2.068(7) Å]. The complex is mononuclear and features a square pyramidal indium (τ_5 = 0.28).

The indium−ligand and indium−alkoxide bond lengths are closely related to those of **LInO^{t}Bu** [In−O = 2.023(6) Å]. The crystal lattice also contains a second uncoordinated diol molecule, which is hydrogen bonded to the indium−alkoxide (Figure S68). It is proposed that during propagation, carbon dioxide inserts into an indium−alkoxide bond to form an indium carbonate intermediate. Thus, the reaction between **LInO^{t}Bu** and CO_2 (1 bar) was monitored using multinuclear NMR spectroscopy (d_8-THF). As soon as carbon dioxide was added to the solution, the $^{13}C\{^1H\}$ NMR spectrum showed a new signal at 164.9 ppm, which is consistent with the formation of an indium−carbonate complex (Figure S69). The $^{31}P\{^1H\}$ NMR spectrum shows a singlet at 38.6 ppm (**$LInO_2CO^tBu$**), which is shifted as compared to that for the alkoxide at 40.3 ppm (**LInO^{t}Bu**). The ^1H NMR spectrum shows signals for the phosphasalen ligand and a singlet at 1.13 ppm assigned to the *tert*-butyl groups; this latter resonance is significantly shifted as compared to the alkoxide precursor (**LInO^{t}Bu**: 0.97 ppm) (Figure S70). When the ^1H NMR spectra of the alkoxide and carbonate intermediates are compared (C_6D_6), clear differences are observed in the aromatic regions: for **LInO^{t}Bu** two distinct *ortho*-phenyl resonances are observed at 7.75, 7.45 ppm, whereas the putative carbonate complex **$LInO_2CO^tBu$** shows only a broad signal at 7.64 ppm for the same protons. The ^1H NMR data are consistent with a change from pentacoordiante indium alkoxide complex to an octahedral indium carbonate complex (Figure S71). Prolonged drying of **$LInO_2CO^tBu$** under vacuum did not result in any changes to the NMR spectra. These data indicate that indium carbonate formation is rapid and irreversible. The indium carbonate complex formation was also investigated using in situ ATR-FTIR spectroscopy. **LInO^{t}Bu** was dissolved in THF, and 1 bar pressure of CO_2 was added, which resulted in the immediate formation of two new signals in the carbonyl region at 1560 and 1400 cm^{-1} (Figure 6). The signals are assigned to asymmetric and symmetric carbonate stretching modes.[99] The stretching frequencies are different from those of a carbonate

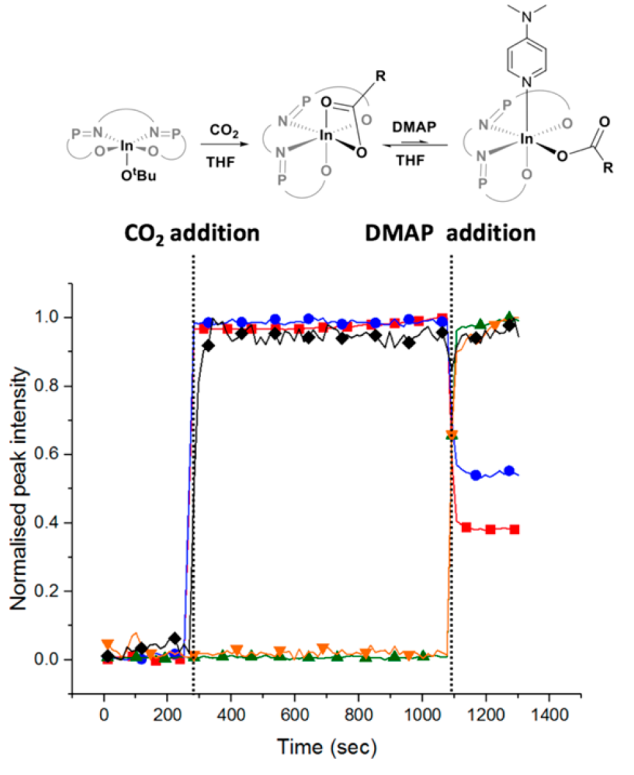

Figure 6. Evolution of selected, normalized IR absorptions against time during the reaction of **LInO^{t}Bu** with (1) carbon dioxide and (2) DMAP. Reaction conditions: (1) **LInO^{t}Bu** (0.1 M), THF, CO_2 (1 bar); (2) DMAP (0.2 M). Absorptions are monitored at 2346 cm^{-1} (CO_2, ◆), 1607 cm^{-1} (DMAP, green ▲), 1387−1410 cm^{-1} (symmetric C−O stretch, red ■), 1559−1574 cm^{-1} (asymmetric C−O stretch, blue ●), and 1618 cm^{-1} (terminal C−O stretch, orange ▼).

DOI: 10.1021/jacs.8b01920
J. Am. Chem. Soc. 2018, 140, 6893−6903

anion (1415 and 1570 cm^{-1}), which suggests speciation as a covalent indium carbonate complex. The IR data can also inform the carbonate coordination modes; metal carboxylate complexes show a difference between asymmetric and symmetric carbonyl stretches (Δ), which indicate the coordination mode: Δ < 200 cm^{-1} is observed for κ^2-chelation, while Δ > 200 cm^{-1} is typical of κ^1-coordination.[99] **LInO$_2$CO^{t}Bu** shows Δ = 160 cm^{-1}, which together with the NMR data indicates κ^2 carbonate chelation.

The rate of formation of **LInO$_2$CO^{t}Bu** is too fast to analyze by NMR spectroscopy (as the reaction is complete prior to the first scan being collected), but can be estimated using ATR-FTIR spectroscopy by analysis of the rate of growth of the signals at 1400 and 1560 cm^{-1}. A control experiment to determine the rate of carbon dioxide dissolution in THF was conducted by monitoring the evolution of the signal at 2346 cm^{-1} assigned to the CO_2 asymmetric stretch. The rates of carbon dioxide dissolution and insertion are nearly identical, which suggests that CO_2 insertion into the indium−alkoxide bond is likely diffusion limited under these experimental conditions (Figure S72).[100]

An indium carbonate complex was isolated from an attempted copolymerization of propylene oxide (PO) and CO_2. **LInO^{t}Bu** was inactive for PO/CO_2 copolymerization (0.1 mol % catalyst, 60 °C, 20 bar CO_2), but after the reaction a white crystalline powder, insoluble in propylene oxide, was isolated. Single-crystal X-ray diffraction experiments show the formation of a dimeric complex (Figures S73 and 74). The structure shows two octahedral indium centers bridged by 1,2-propane dicarbonate. Each indium center is coordinated by a phosphasalen ligand, with a *cis-β* configuration, and by a κ^2-carbonate group with delocalized charge [C−O distances: 1.220(6), 1.264(6) Å]. The solid-state IR and ^{1}H NMR spectra ($CDCl_3$) are also consistent with the solid-state molecular structure. The IR spectrum shows Δ = 152 cm^{-1} indicating chelating carbonate coordination, and the ^{1}H NMR spectrum shows two broadened resonances for the phosphorus phenyl substituents consistent with hexacoordinate indium centers (Figures S75 and S76).

The structure is proposed to form by carbon dioxide insertion into two indium alkoxide groups, with the alkoxides resulting from reaction of the complex with 1,2-propanediol presumably in a manner somewhat analogous to the formation of **LInCHD**. In this case, both alcohol moieties of 1,2-propanediol react with two molecules of **LInO^{t}Bu** so as to form an alkoxide bridged dimer, which is exactly in line with the proposed chain transfer mechanism (see Discussion). It is very unusual to be able to trap such an intermediate and is likely only possible here due to its insolubility and lack of further catalytic activity. It is worth comment that, although a dimeric carbonate intermediate structure is isolated, this does not indicate a bimetallic mechanism because CO_2 insertion reactions (and alcohol chain transfer reactions) happen at both indium centers; that is, chain propagation occurs independently at each indium and does not require cooperativity by two indium atoms during insertion.

Epoxide coordination by the indium carbonate intermediate is another key polymerization reaction. To model coordination in the absence of any subsequent insertion, the reaction of DMAP with **LInCO$_2$O^{t}Bu** was investigated by in situ ATR-IR spectroscopy (Figure 6). The addition of DMAP to the solution of **LInCO$_2$O^{t}Bu** caused an immediate decrease in intensity of the two carbonate resonances, at 1560 and 1400 cm^{-1}, and the appearance of a new signal at 1618 cm^{-1}, assigned to a κ^1 carbonate asymmetric stretch (Δ_{max} = 218 cm^{-1}). There was no evidence of any carbonate dissociation to form carbonate anion. The IR spectra did not change further over ∼1 h of reaction. The final product shows three carbonate stretches (1618, 1560, 1400 cm^{-1}), which is consistent with an equilibrium between two carbonate intermediates, both of octahedral coordination geometry: one with a chelating κ^2-carbonate ligand and the other featuring coordinated DMAP and a terminal κ^1-carbonate ligand (Figure 5).

VT-^{1}H NMR spectroscopy was also used to monitor DMAP coordination (d_8-THF, Figure S77). The addition of 2.5 equiv of DMAP to [**LInO$_2$CO^{t}Bu**] did not change its ^{1}H NMR spectrum at 298 K, but when the solution was cooled to 190 K, DMAP coordination was indicated. At low temperatures, the DMAP phenyl resonances shift from 8.11 to 8.28 ppm and from 6.54 to 5.94 ppm, respectively, while the di(methyl)amine resonance shifts from 2.97 to 2.90 ppm. Integration of the signals suggests quantitative formation of the adduct **LInO$_2$CO^{t}Bu·DMAP**. When the cooled solution was allowed to warm to 298 K, the initial spectrum reformed (i.e., without any evidence of DMAP coordination). The in situ ATR-IR and NMR data are consistent with an equilibrium between **LInO$_2$CO^{t}Bu** and **LInO$_2$CO^{t}Bu·DMAP**. DOSY NMR spectroscopy (298 K) showed mixing of the DMAP and **LInO$_2$CO^{t}Bu** diffusion rates, in line with a rapid equilibrium (Figure S78).[101,102]

DISCUSSION

The structure−activity, kinetic, and catalytic intermediate data are together indicative of an unexpected mononuclear pathway (Figure 7). This mechanism is quite different from the bimetallic or bicomponent mechanisms adopted by the well-

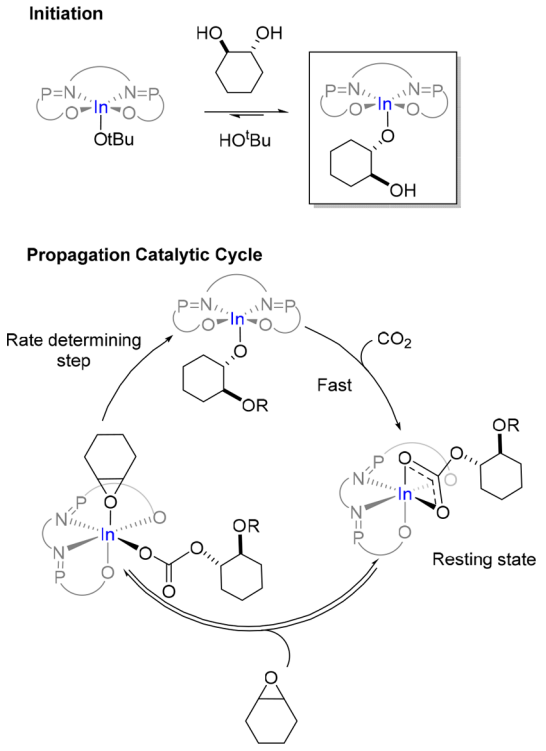

Figure 7. Proposed mononuclear mechanism for CO_2/epoxide ROCOP using indium catalysts. R = growing polymer chain.

DOI: 10.1021/jacs.8b01920
J. Am. Chem. Soc. 2018, 140, 6893−6903

known metal salen catalysts (Figure 1). Given the unusual mechanism, it is appropriate to compare and discuss the key steps and intermediates involved in the catalytic cycle.

Initiation. The indium alkoxide catalysts form polymer chains that are exclusively α,ω-dihydroxyl end-capped, that is, hydroxyl-telechelic polycarbonates, as shown by MALDI-ToF analyses of the polymers (see, for example, Figure S41). The PC molar masses are determined by SEC, calibrated using polystyrene standards, and are only approximate values. Nonetheless, the molar masses are all significantly lower than expected. The formation of lower molar mass, hydroxyl-telechelic polymers is commonly observed with other ROCOP catalysts and is usually ascribed to the presence of 1,2-cyclohexanediol (CHD).[7,34,56,87,91−97] Detailed studies using Cr-salen catalysts established that CHD forms by hydrolysis of cyclohexene oxide and occurs during polymerizations conducted under conditions equivalent to those applied here.[56] It should be noted that ultrahigh purity carbon dioxide (99.999%), purified by flow through two drying columns, was used for all reactions and CHO was fractionally distilled prior to use. Nonetheless, as a dynamic gas atmosphere is applied, low levels of water ingress result in the formation of 1,2-cyclohexanediol. The diol functions as a chain transfer agent and by rapid equilibration with the initiator forms a new transient 1,2-cyclohexanediol alkoxide intermediate, which initiates from both alcohol groups. Here, the indium catalysts operate under conditions where chain transfer is relevant, and, furthermore, the transient catalyst-CHD alkoxide intermediate has been isolated and structurally characterized (Figure 5). Stoichiometric reactivity studies reveal that the alkoxide initiator **^{R}LInO^{t}Bu** (y = ^{t}Bu, amyl, or cumyl) and CHD are in rapid, dynamic equilibrium, which occurs faster than the NMR time-scale. Under polymerization conditions, there is likely excess diol versus catalyst, and thus the true initiator should be the species **LInCHD**. Here, the structure of **LInCHD** is confirmed using X-ray crystallography, and, surprisingly, there are no equivalent structures reported for any metal salen catalysts. In fact, there are only two reports of any related CHD metal complexes. The most relevant, reported by Coates and co-workers, is a dimeric zinc β-diiminate complex with 2-acetoxycyclohexyl-1-alkoxide and acetate bridging ligands, which represents the initiating species formed using acetate ligands but is not relevant to chain transfer.[103] The second is a rhenium alkoxide complex featuring the same monodeprotonated CHD coordination as observed here but that is irrelevant for catalysis.[104] Thus, the isolation and reactivity studies using CHD establish the structure of the key intermediate present during chain transfer (and propagation).

Propagation. **LInCHD** is also an excellent model for the propagating indium alkoxide and reacts equivalently from each alcohol/alkoxide group forming hydroxyl-telechelic polymer chains. **LInCHD**, and by analogy the propagating alkoxide, has pentacoordinate indium in a square-pyramidal coordination geometry, as established by both solid state and solution studies. Even in the presence of excess epoxide and in absence of CO_2, there is no evidence for polyether formation. This lack of reactivity may in part explain the high carbonate linkage selectivity because ether linkages require the reaction of the epoxide with the propagating indium alkoxide intermediate. Rather, during polymerization catalysis, the indium alkoxide intermediate reacts rapidly with carbon dioxide. Indeed, **LInO^{t}Bu** (and by analogy **LInCHD**) reacts very rapidly and irreversibly with carbon dioxide, even at low pressures and under diffusion limited conditions, to form a stable indium carbonate intermediate **LInO$_2$CO^{t}Bu**. The isolated indium carbonate complex models the propagating indium carbonate intermediate and shows a hexacoordinate structure, with octahedral coordination geometry at indium. It features a chelating (κ^2) carbonate and *cis*-β phosphasalen coordination mode. Most salen complexes are proposed to adopt a *trans*-coordination mode, but highly active cobalt salen catalysts also showed *cis*-β configurations.[37,105,106] The extent to which ligand conformation influences reactivity remains uncertain because other cobalt salen complexes adopting *cis*-β ligand configurations are inactive.[37]

Next, in the polymerization pathway, the indium carbonate intermediate coordinates a new epoxide and forms the monomer bound intermediate. Stoichiometric reactions between **LInO$_2$COR** and DMAP indicate that monomer coordination is also an equilibrium reaction. Under polymerization conditions, this equilibrium should be shifted toward adduct because there is an excess of epoxide present (1000 equiv vs catalyst). Adduct formation also changes the carbonate coordination mode, and subsequent propagation is possible at the same metal center from the κ^1-carbonate intermediate. Monomer coordination should occur *cis* to the carbonate group and enables indium carbonate attack and ring-opening to reform an alkoxide intermediate. After epoxide ring-opening, the five-coordinate alkoxide intermediate reforms and the catalytic cycle continues. The catalyst resting state is proposed to be the stable indium carbonate species.

Structure−Activity Studies. Indium phosphasalen complexes show better activity and selectivity than an analogous indium salen complex, which suggests an important ligand effect on catalysis. The phosphasalen ligand is a strong σ and π donor and is more electron donating than an analogous salen ligand.[71,73,107,108] This is relevant to catalysis because the phosphasalen ligands should reduce indium's Lewis acidity and electrophilicity as compared to the salen analogue. The reduced Lewis acidity appears to be beneficial for catalysis, perhaps by increasing the lability of the indium carbonate intermediate through either destabilization of the ground state or stabilization of the transition state. The most active catalysts feature sterically hindered *ortho*-phenolate substituents.

It is tentatively proposed that increasing steric hindrance at the active site may destabilize the hexacoordinate indium carbonate intermediate and favor the formation of the pentacoordinate alkoxide complex (after epoxide ring-opening). Future efforts to model the catalytic cycle and transition states using DFT would be useful to test these hypotheses but are beyond the scope of the current study.

Finally, the moderate activity of indium phosphasalen catalysts may relate to the high stability of the indium carbonate intermediate and the relative proportions of κ^2- versus κ^1-carbonate intermediates. In support of this notion, the crystal structure of the carbonate intermediate (formed by reaction between LInO^{t}Bu/PO/CO_2) shows an additional, uncoordinated propylene oxide molecule in the lattice. This suggests that the chelating carbonate intermediates are sufficiently stable to prevent coordination of this excess epoxide. Future catalyst design strategies should focus on ligand modifications to destabilize the κ^2 carbonate intermediate as this may accelerate epoxide ring-opening and increase catalytic activity.

The isoselectivity exhibited by the phosphasalen catalysts is also unexpected because all other isoselective catalysts are chiral

DOI: 10.1021/jacs.8b01920
J. Am. Chem. Soc. 2018, 140, 6893−6903

and operate by enantiomorphic site control or hybrid mechanisms.[82−84,109−111] Here, the isoselectivity is increased by increasing steric hindrance at the *ortho*-phenolate sites, and stereocontrol occurs by a chain end control mechanism. Recently, the closely related catalyst, ^{cumyl}**LInOEt**, showed high isoselectivity for *rac*-lactide ring-opening polymerization (P_m = 0.92, THF, 298 K); it also operates by a chain end control mechanism.[76] These first findings that chain end control is feasible in ROCOP are important for future efforts to prepare new stereoselective catalysts.

Comparison with Metal Salen Catalysts. Comparing the indium phosphasalen catalysts with the widely studied Cr/Co salen catalysts reveals clear differences in both rate laws and mechanisms. Many metal salen/cocatalyst systems show activities that depend on the carbon dioxide pressure, with turnover frequency values leveling off at pressures between 10 and 30 bar.[27,48,49] There are also reports of bicomponent Co-salen systems, which show very good activities at 1 bar pressure, although in these cases the activity did increase with pressure.[29,34,43] In this work, indium phosphasalen catalysts also show moderate activity at just 1 bar pressure but without any pressure dependence over the range 1−40 bar. The findings are consistent with rapid carbon dioxide insertion and may suggest a different rate-determining step as compared to metal salens. Metal salen catalysts are most effective with equimolar quantities of cocatalyst, preferably PPNX salt (where X = halide or phenolate).[5−7,25,36,52,59] The precise role and speciation during catalysis is likely to be complex; kinetic studies of Cr-salenX/PPNX catalysts reveal orders of 1−1.34 for both catalyst and cocatalyst (∼2−3 equiv of cocatalyst).[40,48,52,53] Two independent kinetic studies of Co-salenX/PPNX systems show orders of 1.57 and 1.61 in catalyst concentration.[42,44] Shortly after the discovery of metal salen ROCOP catalysts, there was an isolated suggestion of a mononuclear mechanism,[44] but detailed subsequent studies using a range of catalysts and epoxides support bicomponent and/or bimetallic mechanisms (Figure 1).[37,40,48,55,56] In contrast, indium phosphasalen catalysts are most active without any cocatalyst and show a clear first-order dependence on catalyst concentration. These findings support a mononuclear mechanism (Figure 6). Further, ionic intermediates are not implicated because the addition of PPNCl as cocatalyst retards the polymerization catalysis and increases formation of the byproduct (cyclic carbonate). The indium carbonate intermediate is stable and yields polymer with very high carbonate linkage content. The in situ IR characterization clearly shows metal−carbonate stretches after coordination of a strong Lewis base, DMAP. These data are consistent with a metal-catalyzed coordination−insertion mechanism without cocatalysts and obviating ionic intermediates. Cocatalysts, and the associated ionic intermediates, are disadvantageous because they are expensive, prone to side-reactions, and result in mixtures of chain end groups, which limits applications as polyols and in polyurethane manufacture.

The ability of indium phosphasalen catalysts to operate by the mononuclear mechanism may relate to an increased ionic radius (r_{ionic} (pm) In(III) = 80; Cr(III) = 62, Co(III) = 55, and Al(III) = 54 pm).[112] The larger indium may be able to accommodate *cis*-coordination of epoxide and carbonate, thereby reducing the barrier to insertion and mononuclear polymerization pathways. Further support for the *cis*-coordination−insertion mechanism comes from the unexpected decrease in catalytic activity when adding a Lewis base cocatalyst. Metal salen catalysts show enhanced activity when used with Lewis base cocatalysts; this is proposed to result from *trans*-coordination by the base, increasing the reactivity of the metal alkoxide bond.[26,48] The mononuclear mechanism is inhibited by Lewis base coordination because it directly competes with epoxide coordination.

The proposed mononuclear mechanism is unexpected in the broader context of other CO_2/epoxide ROCOP catalysts. Generally, dinuclear (or dimeric) Zn(II), Mg(II), and other transition metal complexes show good activity and selectivity.[10,84,113−116] Kinetic and mechanistic studies of these catalysts support bimetallic mechanisms.[23,24,113] Even the heterogeneous metal catalysts, based on zinc glutarate or double metal cyanide surfaces, are proposed to operate with bimetallic cooperativity.[117−119]

CONCLUSIONS

The first indium catalysts for selective carbon dioxide/epoxide ring-opening copolymerization are reported. The catalysts are active at 1 bar pressure of carbon dioxide, enable high carbon dioxide usage, and produce polycarbonate polyols. The phosphasalen ligand is important to the activity as a directly analogous indium salen complex shows inferior performance, and, importantly, the phosphasalen catalysts are most effective without any cocatalyst. The catalysts are also stereocontrolled and produce isotactic polycarbonates by a chain end control mechanism. The findings highlight the need for future ligand design focused on related inexpensive, achiral ligands exploiting the chain end control mechanism. Chiral alkoxide initiators could also be used to further enhance isoselectivity. Catalytic activity and selectivity correlate with increased steric congestion at the metal active site and more electron-donating ligands.

The indium catalysts operate by an unusual mononuclear polymerization pathway, supported by kinetic studies, in situ spectroscopy, and isolated structures of key reaction intermediates. The study affords new insights into the structures and reactivity of the key indium alkoxide and carbonate intermediates; the coordination number and geometries are implicated in relative complex stability and in overall catalytic activity. Further coordination chemistry research is warranted to manipulate equilibria so as to target reactive carbonate intermediates adjacent to vacant sites. It is also likely that other metal catalysts will operate by the mononuclear polymerization pathway, and studies are recommended using larger ionic radii elements from groups 3, 4, 13, and lanthanides. The catalysts and mechanisms reported here may also be relevant to other polymerizations using epoxides, anhydrides, heterocumulenes, and even lactones, enabling the production of stereocontrolled polycarbonates, polyesters, and various block polymers.

ASSOCIATED CONTENT

Supporting Information

The Supporting Information is available free of charge on the ACS Publications website at DOI: 10.1021/jacs.8b01920.

Complete experimental procedures and characterization data for all new compounds and copolymers, and X-ray crystallographic data (PDF)

AUTHOR INFORMATION

Corresponding Author

*charlotte.williams@chem.ox.ac.uk

DOI: 10.1021/jacs.8b01920
J. Am. Chem. Soc. 2018, 140, 6893−6903

ORCID
Charlotte K. Williams: 0000-0002-0734-1575

Notes

The authors declare the following competing financial interest(s): CKW is a director of econic technologies.

■ ACKNOWLEDGMENTS

Funding is acknowledged from EIT, Climate KIC and the Grantham Institute for Climate Change (A.T.), Imperial College London and CSIRO (D.M.), H2020 Marie Curie Fellowship FP7-PEOPLE 2013-IIF (623287) (A.C.), SCG Chemical (C.B.D.), and EPSRC (EP/K014668/1, EP/K035274/1, and EP/L017393/1).

■ REFERENCES

(1) Artz, J.; Muller, T. E.; Thenert, K.; Kleinekorte, J.; Meys, R.; Sternberg, A.; Bardow, A.; Leitner, W. *Chem. Rev.* **2018**, *118* (2), 434−504.
(2) Zhu, Y.; Romain, C.; Williams, C. K. *Nature* **2016**, *540* (7633), 354−362.
(3) Childers, M. I.; Longo, J. M.; Van Zee, N. J.; LaPointe, A. M.; Coates, G. W. *Chem. Rev.* **2014**, *114* (16), 8129−8152.
(4) Poland, S. J.; Darensbourg, D. J. *Green Chem.* **2017**, *19* (21), 4990−5011.
(5) Darensbourg, D. J.; Yeung, A. D. *Polym. Chem.* **2014**, *5* (13), 3949−3962.
(6) Lu, X. B.; Ren, W. M.; Wu, G. P. *Acc. Chem. Res.* **2012**, *45* (10), 1721−1735.
(7) Lu, X. B.; Darensbourg, D. J. *Chem. Soc. Rev.* **2012**, *41* (4), 1462−1484.
(8) Trott, G.; Saini, P. K.; Williams, C. K. *Philos. Trans. R. Soc., A* **2016**, *374*, 20150085.
(9) Romain, C.; Thevenon, A.; Saini, P. K.; Williams, C. K.; Lu, X. B. *Top. Organomet. Chem.* **2015**, *53*, 101−141.
(10) Chapman, A. M.; Keyworth, C.; Kember, M. R.; Lennox, A. J. J.; Williams, C. K. *ACS Catal.* **2015**, *5* (3), 1581−1588.
(11) Darensbourg, D. J.; Chung, W.-C.; Wang, K.; Zhou, H.-C. *ACS Catal.* **2014**, *4* (5), 1511−1515.
(12) Paul, S.; Zhu, Y.; Romain, C.; Brooks, R.; Saini, P. K.; Williams, C. K. *Chem. Commun.* **2015**, *51* (30), 6459−6479.
(13) Korashvili, R.; Nornberg, B.; Bornholdt, N.; Borchardt, E.; Luinstra, G. A. *Chem. Ing. Tech.* **2013**, *85* (4), 437−446.
(14) Luinstra, G. A. *Polym. Rev.* **2008**, *48* (1), 192−219.
(15) Lee, S. H.; Cyriac, A.; Jeon, J. Y.; Lee, B. Y. *Polym. Chem.* **2012**, *3* (5), 1215−1220.
(16) von der Assen, N.; Bardow, A. *Green Chem.* **2014**, *16* (6), 3272−3280.
(17) Assen, N. v. d.; Sternberg, A.; Katelhon, A.; Bardow, A. *Faraday Discuss.* **2015**, *183* (0), 291−307.
(18) Alagi, P.; Ghorpade, R.; Choi, Y. J.; Patil, U.; Kim, I.; Baik, J. H.; Hong, S. C. *ACS Sustainable Chem. Eng.* **2017**, *5* (5), 3871−3881.
(19) Hauenstein, O.; Reiter, M.; Agarwal, S.; Rieger, B.; Greiner, A. *Green Chem.* **2016**, *18* (3), 760−770.
(20) Hauenstein, O.; Agarwal, S.; Greiner, A. *Nat. Commun.* **2016**, *7*, 11862.
(21) Li, C.; Sablong, R. J.; Koning, C. E. *Angew. Chem., Int. Ed.* **2016**, *55* (38), 11572−11576.
(22) Stoesser, T.; Li, C.; Unruangsri, J.; Saini, P. K.; Sablong, R. J.; Meier, M. A. R.; Williams, C. K.; Koning, C. *Polym. Chem.* **2017**, *8* (39), 6099−6105.
(23) Jutz, F.; Buchard, A.; Kember, M. R.; Fredriksen, S. B.; Williams, C. K. *J. Am. Chem. Soc.* **2011**, *133* (43), 17395−17405.
(24) Buchard, A.; Jutz, F.; Kember, M. R.; White, A. J. P.; Rzepa, H. S.; Williams, C. K. *Macromolecules* **2012**, *45* (17), 6781−6795.
(25) Darensbourg, D. J. *Chem. Rev.* **2007**, *107* (6), 2388−2410.
(26) Darensbourg, D. J.; Yarbrough, J. C. *J. Am. Chem. Soc.* **2002**, *124* (22), 6335−6342.
(27) Qin, Z. Q.; Thomas, C. M.; Lee, S.; Coates, G. W. *Angew. Chem., Int. Ed.* **2003**, *42* (44), 5484−5487.
(28) Cohen, C. T.; Chu, T.; Coates, G. W. *J. Am. Chem. Soc.* **2005**, *127* (31), 10869−10878.
(29) Lu, X. B.; Shi, L.; Wang, Y. M.; Zhang, R.; Zhang, Y. J.; Peng, X. J.; Zhang, Z. C.; Li, B. *J. Am. Chem. Soc.* **2006**, *128* (5), 1664−1674.
(30) Cohen, C. T.; Coates, G. W. *J. Polym. Sci., Part A: Polym. Chem.* **2006**, *44* (17), 5182−5191.
(31) Cohen, C. T.; Thomas, C. M.; Peretti, K. L.; Lobkovsky, E. B.; Coates, G. W. *Dalton Trans.* **2006**, No. 1, 237−249.
(32) Nakano, K.; Kamada, T.; Nozaki, K. *Angew. Chem., Int. Ed.* **2006**, *45* (43), 7274−7277.
(33) Noh, E. K.; Na, S. J.; Sujith, S.; Kim, S. W.; Lee, B. Y. *J. Am. Chem. Soc.* **2007**, *129* (26), 8082−8083.
(34) Nakano, K.; Nakamura, M.; Nozaki, K. *Macromolecules* **2009**, *42* (18), 6972−6980.
(35) Nakano, K.; Hashimoto, S.; Nozaki, K. *Chem. Sci.* **2010**, *1* (3), 369−373.
(36) Ren, W. M.; Wu, G. P.; Lin, F.; Jiang, J. Y.; Liu, C.; Luo, Y.; Lu, X. B. *Chem. Sci.* **2012**, *3* (6), 2094−2102.
(37) Jeon, J. Y.; Lee, J. J.; Varghese, J. K.; Na, S. J.; Sujith, S.; Go, M. J.; Lee, J.; Ok, M. A.; Lee, B. Y. *Dalton Trans.* **2013**, *42* (25), 9245−9254.
(38) Liu, Y.; Ren, W. M.; Liu, C.; Fu, S.; Wang, M.; He, K. K.; Li, R. R.; Zhang, R.; Lu, X. B. *Macromolecules* **2014**, *47* (22), 7775−7788.
(39) Liu, Y.; Ren, W. M.; Zhang, W. P.; Zhao, R. R.; Lu, X. B. *Nat. Commun.* **2015**, *6*, 8.
(40) Darensbourg, D. J.; Yeung, A. D. *Polym. Chem.* **2015**, *6* (7), 1103−1117.
(41) Hatazawa, M.; Nakabayashi, K.; Ohkoshi, S.; Nozaki, K. *Chem. - Eur. J.* **2016**, *22* (38), 13677−13681.
(42) Ohkawara, T.; Suzuki, K.; Nakano, K.; Mori, S.; Nozaki, K. *J. Am. Chem. Soc.* **2014**, *136* (30), 10728−10735.
(43) Ren, W. M.; Liu, Z. W.; Wen, Y. Q.; Zhang, R.; Lu, X. B. *J. Am. Chem. Soc.* **2009**, *131* (32), 11509−11518.
(44) Liu, J.; Ren, W. M.; Liu, Y.; Lu, X. B. *Macromolecules* **2013**, *46* (4), 1343−1349.
(45) Vagin, S. I.; Reichardt, R.; Klaus, S.; Rieger, B. *J. Am. Chem. Soc.* **2010**, *132* (41), 14367−14369.
(46) Eberhardt, R.; Allmendinger, M.; Rieger, B. *Macromol. Rapid Commun.* **2003**, *24* (2), 194−196.
(47) Darensbourg, D. J.; Mackiewicz, R. M.; Phelps, A. L.; Billodeaux, D. R. *Acc. Chem. Res.* **2004**, *37* (11), 836−844.
(48) Darensbourg, D. J.; Mackiewicz, R. M. *J. Am. Chem. Soc.* **2005**, *127* (40), 14026−14038.
(49) Darensbourg, D. J.; Mackiewicz, R. M.; Billodeaux, D. R. *Organometallics* **2005**, *24* (1), 144−148.
(50) Darensbourg, D. J.; Phelps, A. L. *Inorg. Chem.* **2005**, *44* (13), 4622−4629.
(51) Darensbourg, D. J.; Frantz, E. B. *Dalton Trans.* **2008**, *37*, 5031−5036.
(52) Darensbourg, D. J.; Moncada, A. I. *Inorg. Chem.* **2008**, *47* (21), 10000−10008.
(53) Darensbourg, D. J.; Moncada, A. I.; Choi, W.; Reibenspies, J. H. *J. Am. Chem. Soc.* **2008**, *130* (20), 6523−6533.
(54) Darensbourg, D. J.; Ulusoy, M.; Karroonnirum, O.; Poland, R. R.; Reibenspies, J. H.; Cetinkaya, B. *Macromolecules* **2009**, *42* (18), 6992−6998.
(55) Darensbourg, D. J.; Chung, W. C.; Wilson, S. J. *ACS Catal.* **2013**, *3* (12), 3050−3057.
(56) Wu, G. P.; Darensbourg, D. J. *Macromolecules* **2016**, *49* (3), 807−814.
(57) Nishioka, K.; Goto, H.; Sugimoto, H. *Macromolecules* **2012**, *45* (20), 8172−8192.
(58) Darensbourg, D. J.; Billodeaux, D. R. *Inorg. Chem.* **2005**, *44* (5), 1433−1442.
(59) Fieser, M. E.; Sanford, M. J.; Mitchell, L. A.; Dunbar, C. R.; Mandal, M.; Van Zee, N. J.; Urness, D. M.; Cramer, C. J.; Coates, G. W.; Tolman, W. B. *J. Am. Chem. Soc.* **2017**, *139* (42), 15222−15231.

DOI: 10.1021/jacs.8b01920
J. Am. Chem. Soc. 2018, 140, 6893−6903

(60) Nielsen, L. P. C.; Zuend, S. J.; Ford, D. D.; Jacobsen, E. N. *J. Org. Chem.* **2012**, *77* (5), 2486−2495.
(61) Ford, D. D.; Nielsen, L. P. C.; Zuend, S. J.; Musgrave, C. B.; Jacobsen, E. N. *J. Am. Chem. Soc.* **2013**, *135* (41), 15595−15608.
(62) Xia, W.; Salmeia, K. A.; Vagin, S. I.; Rieger, B. *Chem. - Eur. J.* **2015**, *21* (11), 4384−4390.
(63) Shibata, I.; Mitani, I.; Imakuni, A.; Baba, A. *Tetrahedron Lett.* **2011**, *52* (6), 721−723.
(64) Xu, L.; Zhai, M. K.; Lu, X. C.; Du, H. B. *Dalton Trans.* **2016**, *45* (46), 18730−18736.
(65) Weidlein, J. *Z. Anorg. Allg. Chem.* **1970**, *378* (3), 245−262.
(66) Cocolios, P.; Guilard, R.; Bayeul, D.; Lecomte, C. *Inorg. Chem.* **1985**, *24* (13), 2058−2062.
(67) Aluthge, D. C.; Patrick, B. O.; Mehrkhodavandi, P. *Chem. Commun.* **2013**, *49* (39), 4295−4297.
(68) Maudoux, N.; Roisnel, T.; Dorcet, V.; Carpentier, J.-F.; Sarazin, Y. *Chem. - Eur. J.* **2014**, *20* (20), 6131−6147.
(69) Kremer, A. B.; Andrews, R. J.; Milner, M. J.; Zhang, X. R.; Ebrahimi, T.; Patrick, B. O.; Diaconescu, P. L.; Mehrkhodavandi, P. *Inorg. Chem.* **2017**, *56* (3), 1375−1385.
(70) Cao, T. P. A.; Labouille, S.; Auffrant, A.; Jean, Y.; Le Goff, X. F.; Le Floch, P. *Dalton Trans.* **2011**, *40* (39), 10029−10037.
(71) Cao, T. P. A.; Nocton, G.; Ricard, L.; Le Goff, X. F.; Auffrant, A. *Angew. Chem., Int. Ed.* **2014**, *53* (5), 1368−1372.
(72) Garcia-Alvarez, J.; Garcia-Garrido, S. E.; Cadierno, V. *J. Organomet. Chem.* **2014**, *751*, 792−808.
(73) Bakewell, C.; Cao, T. P. A.; Le Goff, X. F.; Long, N. J.; Auffrant, A.; Williams, C. K. *Organometallics* **2013**, *32* (5), 1475−1483.
(74) Bakewell, C.; White, A. J. P.; Long, N. J.; Williams, C. K. *Angew. Chem., Int. Ed.* **2014**, *53* (35), 9226−9230.
(75) Bakewell, C.; White, A. J. P.; Long, N. J.; Williams, C. K. *Inorg. Chem.* **2015**, *54* (5), 2204−2212.
(76) Myers, D.; White, A. J. P.; Forsyth, C. M.; Bown, M.; Williams, C. K. *Angew. Chem., Int. Ed.* **2017**, *56* (19), 5277−5282.
(77) Addison, A. W.; Rao, T. N.; Reedijk, J.; van Rijn, J.; Verschoor, G. C. *J. Chem. Soc., Dalton Trans.* **1984**, *7*, 1349−1356.
(78) Yu, I.; Acosta-Ramirez, A.; Mehrkhodavandi, P. *J. Am. Chem. Soc.* **2012**, *134* (30), 12758−12773.
(79) Fang, J.; Yu, I. S.; Mehrkhodavandi, P.; Maron, L. *Organometallics* **2013**, *32* (23), 6950−6956.
(80) Aluthge, D. C.; Yan, E. X.; Ahn, J. M.; Mehrkhodavandi, P. *Inorg. Chem.* **2014**, *53* (13), 6828−6836.
(81) Aluthge, D. C.; Ahn, J. M.; Mehrkhodavandi, P. *Chem. Sci.* **2015**, *6* (9), 5284−5292.
(82) Nakano, K.; Nozaki, K.; Hiyama, T. *J. Am. Chem. Soc.* **2003**, *125* (18), 5501−5510.
(83) Nakano, K.; Hiyama, T.; Nozaki, K. *Chem. Commun.* **2005**, *14*, 1871−1873.
(84) Ellis, W. C.; Jung, Y.; Mulzer, M.; Di Girolamo, R.; Lobkovsky, E. B.; Coates, G. W. *Chem. Sci.* **2014**, *5* (10), 4004−4011.
(85) Bovey, F. A. *Pure Appl. Chem.* **1967**, *15* (3−4), 349−368.
(86) Sepulchre, M. *Makromol. Chem.* **1988**, *189* (5), 1117−1131.
(87) Kember, M. R.; Knight, P. D.; Reung, P. T. R.; Williams, C. K. *Angew. Chem., Int. Ed.* **2009**, *48* (5), 931−933.
(88) Ikpo, N.; Flogeras, J. C.; Kerton, F. M. *Dalton Trans.* **2013**, *42* (25), 8998−9006.
(89) Reiter, M.; Vagin, S.; Kronast, A.; Jandl, C.; Rieger, B. *Chem. Sci.* **2017**, *8* (3), 1876−1882.
(90) Sujith, S.; Min, J. K.; Seong, J. E.; Na, S. J.; Lee, B. Y. *Angew. Chem., Int. Ed.* **2008**, *47* (38), 7306−7309.
(91) Lee, B. Y.; Kwon, H. Y.; Lee, S. Y.; Na, S. J.; Han, S.-i.; Yun, H.; Lee, H.; Park, Y.-W. *J. Am. Chem. Soc.* **2005**, *127* (9), 3031−3037.
(92) Sugimoto, H.; Kuroda, K. *Macromolecules* **2008**, *41* (2), 312−317.
(93) Nakano, K.; Kobayashi, K.; Nozaki, K. *J. Am. Chem. Soc.* **2011**, *133* (28), 10720−10723.
(94) Kember, M. R.; Williams, C. K. *J. Am. Chem. Soc.* **2012**, *134* (38), 15676−15679.
(95) Nakano, K.; Kobayashi, K.; Ohkawara, T.; Imoto, H.; Nozaki, K. *J. Am. Chem. Soc.* **2013**, *135* (23), 8456−8459.
(96) Kember, M. R.; Copley, J.; Buchard, A.; Williams, C. K. *Polym. Chem.* **2012**, *3* (5), 1196−1201.
(97) Decortes, A.; Haak, R. M.; Martin, C.; Belmonte, M. M.; Martin, E.; Benet-Buchholz, J.; Kleij, A. W. *Macromolecules* **2015**, *48* (22), 8197−8207.
(98) Oikonomou, M.; Asencio-Hernández, J.; Velders, A. H.; Delsuc, M.-A. *J. Magn. Reson.* **2015**, *258* (Supplement C), 12−16.
(99) Deacon, G. B.; Phillips, R. J. *Coord. Chem. Rev.* **1980**, *33* (3), 227−250.
(100) Brown, N. J.; Harris, J. E.; Yin, X.; Silverwood, I.; White, A. J. P.; Kazarian, S. G.; Hellgardt, K.; Shaffer, M. S. P.; Williams, C. K. *Organometallics* **2014**, *33* (5), 1112−1119.
(101) Aguilar, J. A.; Adams, R. W.; Nilsson, M.; Morris, G. A. *J. Magn. Reson.* **2014**, *238* (Supplement C), 16−19.
(102) Johnson, C. S. *Prog. Nucl. Magn. Reson. Spectrosc.* **1999**, *34* (3), 203−256.
(103) Moore, D. R.; Cheng, M.; Lobkovsky, E. B.; Coates, G. W. *J. Am. Chem. Soc.* **2003**, *125* (39), 11911−11924.
(104) Hinrichs, M.; Hofbauer, F. R.; Klüfers, P. *Chem. - Eur. J.* **2006**, *12* (17), 4675−4683.
(105) Na, S. J.; Sujith, S.; Cyriac, A.; Kim, B. E.; Yoo, J.; Kang, Y. K.; Han, S. J.; Lee, C.; Lee, B. Y. *Inorg. Chem.* **2009**, *48* (21), 10455−10465.
(106) Cyriac, A.; Jeon, J. Y.; Varghese, J. K.; Park, J. H.; Choi, S. Y.; Chung, Y. K.; Lee, B. Y. *Dalton Trans.* **2012**, *41* (5), 1444−1447.
(107) Cao, T. P. A.; Buchard, A.; Le Goff, X. F.; Auffrant, A.; Williams, C. K. *Inorg. Chem.* **2012**, *51* (4), 2157−2169.
(108) Bézier, D.; Daugulis, O.; Brookhart, M. *Organometallics* **2017**, *36* (15), 2947−2951.
(109) Liu, Y.; Ren, W.-M.; He, K.-K.; Lu, X.-B. *Nat. Commun.* **2014**, *5*, 5687.
(110) Nozaki, K.; Nakano, K.; Hiyama, T. *J. Am. Chem. Soc.* **1999**, *121* (47), 11008−11009.
(111) Liu, Y.; Ren, W.-M.; Liu, J.; Lu, X.-B. *Angew. Chem., Int. Ed.* **2013**, *52* (44), 11594−11598.
(112) Shannon, R. *Acta Crystallogr., Sect. A: Cryst. Phys., Diffr., Theor. Gen. Crystallogr.* **1976**, *32* (5), 751−767.
(113) Lehenmeier, M. W.; Kissling, S.; Altenbuchner, P. T.; Bruckmeier, C.; Deglmann, P.; Brym, A. K.; Rieger, B. *Angew. Chem., Int. Ed.* **2013**, *52* (37), 9821−9826.
(114) Kember, M. R.; Jutz, F.; Buchard, A.; White, A. J. P.; Williams, C. K. *Chem. Sci.* **2012**, *3* (4), 1245−1255.
(115) Kissling, S.; Lehenmeier, M. W.; Altenbuchner, P. T.; Kronast, A.; Reiter, M.; Deglmann, P.; Seemann, U. B.; Rieger, B. *Chem. Commun.* **2015**, *51* (22), 4579−4582.
(116) Garden, J. A.; Saini, P. K.; Williams, C. K. *J. Am. Chem. Soc.* **2015**, *137* (48), 15078−15081.
(117) Ree, M.; Bae, J. Y.; Jung, J. H.; Shin, T. J. *J. Polym. Sci., Part A: Polym. Chem.* **1999**, *37* (12), 1863−1876.
(118) Kim, I.; Yi, M. J.; Lee, K. J.; Park, D. W.; Kim, B. U.; Ha, C. S. *Catal. Today* **2006**, *111* (3−4), 292−296.
(119) Marbach, J.; Nornberg, B.; Rahlf, A. F.; Luinstra, G. A. *Catal. Sci. Technol.* **2017**, *7* (13), 2897−2905.

DOI: 10.1021/jacs.8b01920
J. Am. Chem. Soc. 2018, 140, 6893−6903